# A Numerical Analysis of Reaction-Diffusion Effects on Species Mixing Rates in Turbulent Premixed Methane-Air Combustion

E.S.Richardson[a,*], R.Sankaran[b], R.W. Grout[a], J.H. Chen[a]

[a] Reacting Flow Research Department, Combustion Research Facility, Sandia National Laboratories, Livermore, CA 94551-0969

[b] National Center for Computational Sciences, Oak Ridge National Laboratory, Oak Ridge, TN 37831-6008

**Abstract**

Reactive scalar mixing time scale have been investigated in direct numerical simulation data for turbulent premixed Bunsen flames with reduced methane-air chemistry. Previous conclusions from single step chemistry studies are confirmed regarding the role of dilatation and turbulence-chemistry interactions on the progress variable dissipation rate. Compared to the progress variable, the mixing rates of intermediate species can be several times greater. The variation of species mixing rates are explained with reference to the structure of one-dimensional flamelets. A new model is produced for the ratios of scalar mixing time scales which can be applied, for example, in transported probability density function simulations.

## Introduction

Predictive models for turbulent premixed and partially premixed combustors are of increasing practical interest. The trend towards more dilute combustion in gas turbines, reciprocating engines and other burners limit the scope for high Damköhler number approaches. Advanced turbulent reactive flow models which may be necessary for practical applications typically require turbulent mixing frequencies or dissipation rates. In the transported probability density function (PDF) approach [1, 2], for example, the chemical reaction rate appears in closed form and closure must be achieved by modeling the molecular mixing processes.

The scalar dissipation rate for species mass fraction $Y_i$ and its turbulent mixing time scale $\tau_i^{-1}$ are given in Eq. 1 and Eq. 2,

$$\overline{\rho}\tilde{\epsilon}_i = \overline{\rho D_i \nabla Y_i'' . \nabla Y_i''} \tag{1}$$

$$\tau_i^{-1} = \tilde{\epsilon}_i / \widetilde{Y_i'' Y_i''}, \tag{2}$$

$\rho$ is density, D is molecular diffusivity, and $Y_i''$ is the fluctuation about the Favre average $\tilde{Y}_i$. At high Reynolds number, the rate of scalar variance decay is strongly dependent on the large scales of the turbulence [3]. In addition, species gradients are affected by reaction and diffusion processes. Where reaction-diffusion generated species gradients persist at high Reynolds number, such as in the flamelet combustion regime, a range of mixing frequencies may be expected among the different species. More generally, mixing models using a single turbulence parameter are unable to capture effects of preferential diffusion or dependence on the length scales of the scalar fields [4, 5]. Despite the possibility of differing mixing rates, PDF mixing models commonly assume all scalars mix at the same rate [6, 7].

The customary closure of the scalar dissipation time scale is to scale it with the integral turbulent timescale,

$$\tau_i^{-1} = \frac{C_\phi}{2}\frac{\epsilon}{k} = \frac{C_\phi}{2}\tau_t^{-1}, \tag{3}$$

where $\epsilon$ is the dissipation rate of turbulent kinetic energy $k$ [8] and $C_\phi$ is an empirical constant. Closures for the scalar dissipation rate also have been derived based on its transport equation, by Zeman and Lumley [9], Jones and Musonge [10], and Mantel and Borghi [11], among others.

The transport equation for the Favre averaged dissipation rate presented by Swaminathan and Bray [12] is written below for species $i$, Eq. 4.

$$\begin{aligned} &\tfrac{\partial \overline{\rho}\tilde{\epsilon}_i}{\partial t} + \tfrac{\partial}{\partial x_j}\left(\overline{\rho}\tilde{u}_j\tilde{\epsilon}_i\right) - \tfrac{\partial}{\partial x_j}\left(\overline{\rho D_i}\tfrac{\partial \tilde{\epsilon}_i}{\partial x_j}\right) + \overline{2\rho {D_i}^2\left(\tfrac{\partial Y_{i,k}''}{\partial x_j}\tfrac{\partial Y_{i,k}''}{\partial x_j}\right)} \\ &= T_1 + T_2 + T_3 + T_4 + O(D_i), \end{aligned} \tag{4}$$

where

$$\begin{aligned} T_1 &\equiv -\tfrac{\partial \overline{\rho u_j'' \epsilon_i}}{\partial x_j} - 2\overline{\rho\alpha}\left(\widetilde{u_j'' Y_{i,k}''}\right)\tfrac{\partial \tilde{Y}_{i,k}}{\partial x_j} = T_{11} + T_{12}, \\ T_2 &\equiv 2D_i\tfrac{\rho_{,k}}{\rho}Y_{i,k}''\left(\omega_i + \tfrac{\partial[\rho D_i Y_{i,j}]}{\partial x_j}\right), \\ T_3 &\equiv -2\overline{\rho D_i}\tilde{Y}_{i,j}\widetilde{Y_{i,k}'' u_{j,k}''} - 2\overline{\rho D_i}\widetilde{Y_{i,j}'' e_{jk}''}Y_{i,k}'' \\ &\quad -2\overline{\rho D_i}\widetilde{Y_{i,j}'' Y_{i,k}''}\widetilde{e_{jk}} \\ &= T_{31} + T_{32} + T_{33}, \\ T_4 &\equiv 2\left(\overline{D_i Y_{i,k}'' \omega_{i,k}''}\right). \end{aligned} \tag{5}$$

In this equation u is velocity; $\omega$ is the chemical production rate; j and k are spatial coordinate indices such that $Y_{i,k}''$ indicates $\partial Y_i''/\partial x_k$. $e_{jk}$ is the stress tensor [8]. Note that this equation approximates fluctuations of gradients by gradients of the fluctuating quantity, $(Y_{,k})'' = (Y'')_{,k}$. This is inexact in variable density flow. The final term, $O(D_i)$, which arises due to transport of species diffusivities, is neglected in the subsequent analysis. These simplifications do not lead to significant imbalance of Eq. 4 in the flames considered in this paper. The left hand side terms represent the temporal and convective changes of $\overline{\rho}\tilde{\epsilon}$,

*Corresponding author: esrich@sandia.gov

its transport, and its dissipation due to molecular diffusion, respectively. Swaminathan and Bray consider the dissipation rate of a premixed flame's progress variable and conducted an order of magnitude analysis of Eq.4's terms using scaling based on laminar flame quantities [12]. This analysis suggests that the dissipation term, dilatation effects $T_2$, turbulence-scalar interaction $T_{32}$, and reaction $T_4$ will show first order scaling with Damköhler number, $Da_c = (S_L.l_t)/(\delta_L.u')$. $S_L$ and $\delta_L$ are the laminar flame speed and thickness, $l_t$ and u' are the integral turbulent length scale and root mean square velocity fluctuations. This implies that the remaining terms will become less important during turbulent combustion in the flamelet regime. In the absence of reaction, scalar gradients are controlled predominantly by a balance of the dissipation term and the enhancement of scalar gradients by compressive strain, $T_{32}$. The flamelet based order of magnitude analysis results in similar Da scalings for the minor flame species with the caveat that the Damköhler numbers can differ vastly among species. The species time scale ratio $Da_i/Da_c=(\omega_i/Y_i)/(\omega_c/c)$ is presented in Table 1. $Da_i/Da_c$ was evaluated in an 800K, 1atm, $\phi$=0.7, strained, planar laminar premixed flame computing the numerator and denominator at the locations of maximum reaction rates $\omega_i$ and $\omega_c$. The tangential strain rate $a_t$ used was $1.5\tau_f^{-1}$, where the characteristic flame time $\tau_f=\delta_L/S_L$. These conditions are representative of the flames studied later in this paper.

Table 1: Lewis numbers and Damköhler number ratios for selected species.

| Species | $O_2$ | CO | OH | $H_2$ | H |
|---|---|---|---|---|---|
| $Le_i$ | 1.08 | 1.07 | 0.70 | 0.29 | 0.17 |
| $Da_i/Da_{O2}$ | 1.0 | 2.7 | 21 | 82 | 510 |

In constant density flows $T_3$ represents the increase of scalar gradients, and hence dissipation rate, by compressive strain aligned with the scalar gradient. The modeling of this term presented by Borghi and coworkers [11, 13], neglecting the other terms of Eq. 4 results in an algebraic model similar to Eq. 3. For premixed turbulent combustion in the flamelet regime thermal expansion in the flame can modify the strain field such that $T_3$ dissipates gradients of progress variable [12, 14, 15, 16, 17]. The relative magnitude of the dilatation effect increases with both the density ratio across the flame and the Damköhler number [15, 17].

By considering the reaction-diffusion balance in premixed flame propagation, Mantel and Borghi [11] showed that the reaction term $T_4$ cancels with part of $T_3$ corresponding to dissipation in the direction normal to the flame. The remaining portion of $T_3$ is associated with flame curvature. Borghi and coworkers [11, 13] provide modeling for the flame curvature which introduces a dependence of $C_\phi$ on $u'/S_L$. Other studies [18, 19, 20] have indicated that a scaling based on the ratio the Kolmogorov velocity to flame propagation speed better represents the effects of turbulent flame curvature. Assuming that all species profiles in the flame exhibit the same characteristic radius of curvature, Mantel and Borghi's argument maintains that mixing of every high Da species would have the same dependence on flame propagation. This assumption needs to be examined for real flames subject to curvature where preferential diffusion acts to focus species concentrations [21] or in the thin/broken reaction zone regimes in which turbulent eddies penetrate and perturb the reaction-diffusion layers.

Swaminathan and Bray [12] find that $T_2$ provides a source term for the progress variable dissipation rate which is dependent on the dilatation through the flame [22]. The role played by term $T_2$ for intermediate species, whose concentrations do not vary linearly with temperature does not appear to have been studied.

Models designed to account for the different dissipation rates among species have been considered in the context of non-premixed combustion. Chen and Chang [23] account for differential diffusion, effectively adjusting species mixing rates according to their individual diffusion rates in a hypothetical one-dimensional mixing layer. This approach has some success in diffusion flames, but may be limited by its neglect of the effects of reaction on mixing. Cha and Trouillet [24] use the mapping closure for non-premixed combustion (neglecting preferential diffusion) to relate species mixing frequencies to that of mixture fraction. Use of the mapping closure works because, by computing a flamelet solution in the mapping variable space, gradients of mixture fraction can be transformed into gradients of the reactive scalars. While mapping the one-dimensional flame solution onto mixture fraction is promising, extensions of the mapping closure for premixed combustion, or for differential diffusion, do not appear to be available.

**Specific Objectives**

The present work considers the scalar mixing time-scales occurring in premixed methane-air combustion and how they might be modeled for use in transported PDF calculations. Three-dimensional, reduced chemistry DNS data for turbulent premixed Bunsen flames in the thin reaction zones regime [25, 26] have been analyzed to assess previous findings regarding the progress variable dissipation rate which were based on two-dimensional turbulence or single step chemistry. In this work the mixing rates of intermediate species are also analyzed, leading to a model which relates their dissipation rate to that of the progress variable.

**Configuration**

Three-dimensional turbulent, premixed Bunsen flames A and C [27] have been analyzed in this study. The configuration simulated by Sankaran et al. [27, 28] comprises a planar jet of unburned methane and air at 800K, 1atm and equivalence ratio $\phi$=0.7 issuing into a coflowing atmosphere composed of the products from adiabatic combustion of the $\phi$=0.7, 800K mixture. The elevated temperature approximates that seen in some engine applications, meanwhile it is sufficiently low that flameless combustion does not occur. The piloted jet configuration permits high levels of mean shear while ensuring the flame can not blow off. At these conditions the unstrained planar laminar flame speed, $S_L$ is $1.8m^{-1}$, and thermal thickness, $\delta_L$=0.3mm,

Table 2: Simulation parameters. The Karlovitz (Ka) and Damköhler numbers shown were evaluated at $x/L_x$=0.25. Mean tangential strain $a_t$, conditional on c=0.65, is given for three axial locations.

| | Case A | Case C |
|---|---|---|
| Slot width | H=1.2mm | H=1.8mm |
| Jet velocity | $u_j$=60ms$^{-1}$ | $u_j$=100ms$^{-1}$ |
| Coflow velocity | 15ms$^{-1}$ | 25ms$^{-1}$ |
| Domain size $L_x$,$L_y$,$L_z$ | 12H×12H×3H | 13H×12H×3H |
| Ka=$(\alpha/S_L\eta_k)^2$ | 2.3 | 5.2 |
| Da=$(S_L l_t/\delta_L u')$ | 0.23 | 0.15 |
| $a_t\tau_f$, $x/L_x$=0.25 | 2.0 | 4.75 |
| $a_t\tau_f$, $x/L_x$=0.25 | 1.5 | 3.0 |
| $a_t\tau_f$, $x/L_x$=0.25 | 1.25 | 2.25 |

give a flame time scale $\tau_f$=0.17ms. Flame specific parameters are given in Table 2.

Chemical reaction was modeled using a reduced mechanism with low temporal stiffness developed from the detailed GRI-1.2 scheme [29]. Details of the reduction methodology and validation of the reduced mechanism can be found in Ref. [28]. The mixture-averaged thermal conductivity is temperature-dependent [30], and the individual species specific heats are obtained using the CHEMKIN thermodynamic database [31]. The diffusion coefficients are obtained by prescription of Lewis numbers for individual species, fitted from mixture-averaged transport coefficients [31]. A selection of the Lewis numbers used are included in Table 1.

The composition at the inlet plane was specified with reference to a premixed laminar flame solution using a progress variable look-up table. A hyperbolic tangent function was used to obtain a smooth variation of progress variable between the jet and the coflow. A turbulent velocity field was synthesized by specifying the length scale (2H), magnitude of velocity fluctuations ($u_j$/3) and spectral energy density [32]. The resultant velocity field was added to the mean inflow velocity profile of the jet, but not the coflow, and used as the velocity inflow boundary condition based on Taylor's hypothesis.

Navier-Stokes characteristic boundary conditions [33, 34, 35, 36] were used to prescribe the boundary conditions. The boundary conditions were periodic in the spanwise direction (z), non-reflecting inflow and outflow in the streamwise direction (x), and non-reflecting outflow in the transverse direction (y).

The simulations were performed using the DNS code S3D, which solves the fully compressible Navier-Stokes, species and energy equations with a fourth-order Runge-Kutta method for time integration and an eighth-order explicit spatial differencing [37, 38]. A uniform 20$\mu$m grid spacing was employed throughout the volume occupied by the turbulent jet flame. The y-direction grid was stretched algebraically in the laminar coflow. The simulation was advanced with 2ns time steps. Further details of the configuration are given in Refs. [27, 28].

Based on the mean jet velocity and the domain height, all three cases have a jet flow through time of 0.24ms. Only data from after the first flow through time have been analyzed to enable artifacts from the initial condition to gracefully leave the domain. Where averages have been reported, they are evaluated using 61 equally spaced time instants over the course of one flow through time and by integrating over the homogeneous *z*-direction. The conditional averages reported have been evaluated by integrating over the volume $0.2H \times 0.2H \times L_z$, centered upon $x=0.5L_x$, y=0.5H. This y position was chosen since it experiences the full range of progress variable.

**Results and Discussion**

The characteristics of flames A and C have been presented previously [27, 28]. The progress variable used in the subsequent analysis, with c=0 in the reactants and c=1 in the products, varies linearly with $Y_{O_2}$ so that $\tau_c^{-1}=\tau_{O_2}^{-1}$. In summary, wrinkling and flame-flame interactions increase from flame A to flame C. Occurrences of flame pinch-off become significant beyond $x/L_x$=0.5, as seen for case C in Fig. 1. The majority of the flame area is convex towards the products, with cusps orientated towards the reactants. This is contrary to Huygens-type self-propagation, providing evidence that flame topology is strongly influenced by turbulent straining. The simulation Karlovitz numbers, Table 2, and previous analyses [27, 28] indicate that flame C is characterized by the thin reaction zones regime [25, 26], in which turbulent eddies penetrate the flame's preheat layer but are too large to disrupt the reaction zone. Case A shows weaker thickening of the preheat layer and appears to be closer to the corrugated flamelet regime [28]. Figure 1 shows the Favre averaged progress variable field. The mechanical turbulent mixing frequency $\tau_t^{-1}$ and the progress variable mixing frequency $\tau_c^{-1}$ are compared at three axial locations through flame C in Fig. 1. As discussed above, assumption of proportionality between momentum and species mixing rates is generally inaccurate in turbulent premixed combustion. The strong discrepancy that arises towards the edges of the jet, where progress variable and velocity variances become small, may be of limited practical relevance.

The ratio of mixing frequencies $\tau_{CO}^{-1}$, $\tau_{H_2}^{-1}$, $\tau_H^{-1}$ and $\tau_{OH}^{-1}$ to $\tau_{O_2}^{-1}$ are plotted in Fig. 2 for both flames A and C. The cross stream variation is shown at three axial locations as well as plotting the variation against the mean progress variable at $x/L_x$=0.5. Figures 2d,f show double lines, one for each side of the flame. Except for OH the ratios differ markedly from unity, exceeding ten in the case of $H_2$. The most diffusive species H and $H_2$ exhibit the greatest mixing rates, however Lewis number does not appear to be the only consideration since the ratios vary considerably through the flame with the less diffusive $H_2$ mixing faster than H in many regions.

The processes governing the reactive scalar dissipation rates may be investigated with reference to the balance of Eq. 4. The terms contributing to the rate of change of the $O_2$, OH, CO and H scalar dissipation rates are plotted in Fig. 3 for flame C. While the absolute magnitudes differ, the resulting balance for flame A is extremely similar and is not shown. The imbalance of Eq. 4, which is due to limited statistical convergence and approximations in the derivation, is small compared to the dominant terms and is not shown.

In accordance with the order of magnitude analysis of Swaminathan and Bray [12], the dominant processes governing

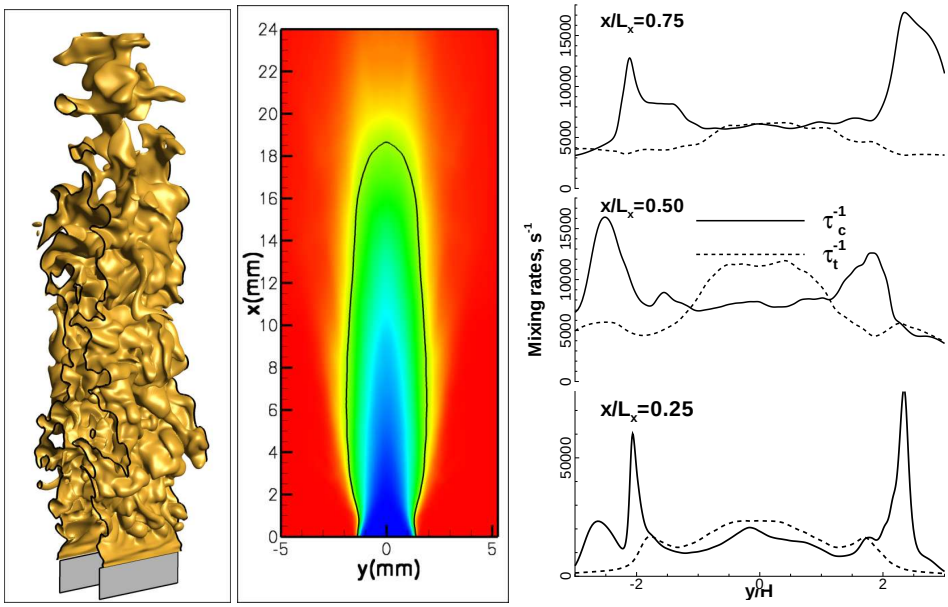


Figure 1: Instantaneous iso-surface of the progress variable (c=0.65) representing the flame surface (left); 2D x-y contours of $\tilde{c}$ with the $\tilde{c}$=0.65 iso-line drawn in black, c=1 (red) in the coflow and c=0 (blue) at the jet nozzle (center); and cross-stream profiles of the progress variable $\tau_c^{-1}$ (solid lines) and mechanical $\tau_t^{-1}$ (dashed) mixing frequencies at three axial positions x/$L_x$=0.25, 0.5, 0.75 (right). Data are for flame C.

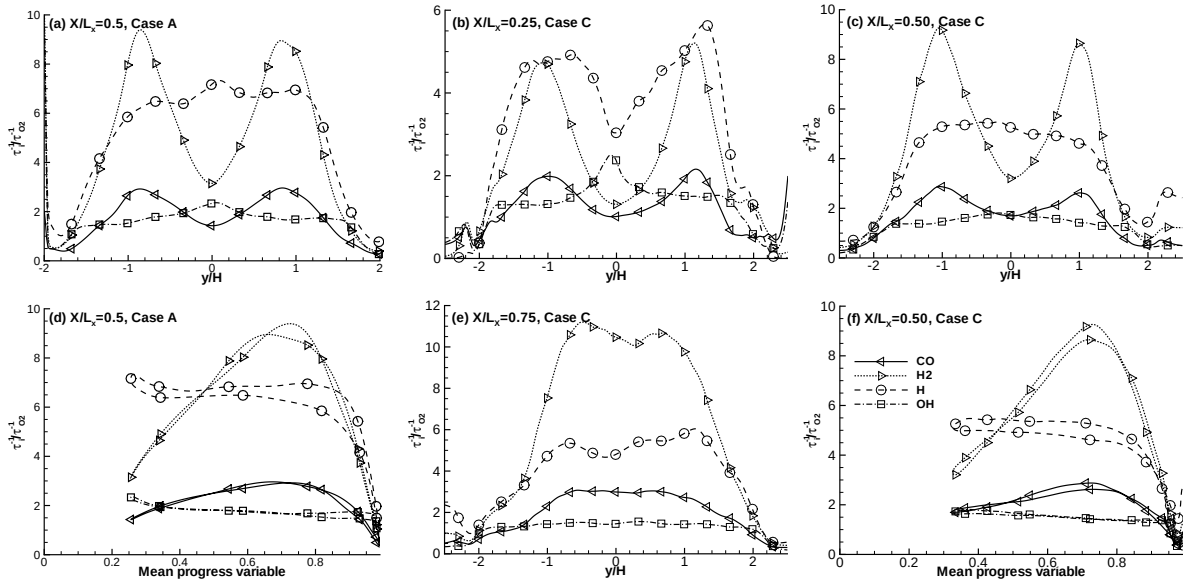


Figure 2: Intermediate species-progress variable time scale ratios showing $\tau_{CO}^{-1}$, $\tau_{H_2}^{-1}$, $\tau_H^{-1}$, and $\tau_{OH}^{-1}$ divided by $\tau_{O_2}^{-1}$. The variation in the cross stream direction is shown for flame A at x/$L_x$=0.5 (a) and for flame C at x/$L_x$=0.25 (b), x/$L_x$=0.5 (c), x/$L_x$=0.75 (e), and versus the mean progress variable at x/$L_x$=0.5 for flame A (d) and flame C (f).

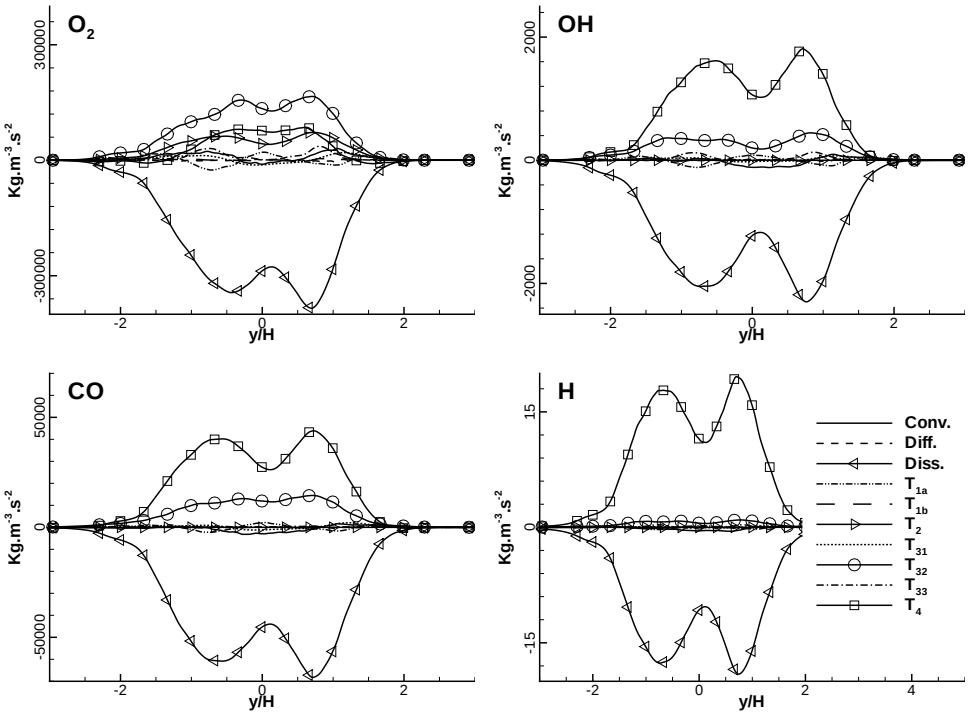


Figure 3: Balance of the scalar dissipation rate Eq. 4 for $O_2$ (a), OH (b), CO (c), H (d). Data are plotted at $x/L_x$=0.5 for flame C.

the $O_2$ dissipation rate are the dilatation $T_2$, turbulence-scalar interaction $T_{32}$ and reaction $T_4$ source terms balancing the dissipation of scalar gradients. The fact that $T_{32}$ acts as a source of $Y_{O_2}$ gradients indicates that at these conditions, the Damköhler number and flame density ratio are sufficiently small that turbulent straining overrides thermal expansion effects [17]. The dilatation term $T_2$ and reaction term $T_4$ have a similar magnitude, approximately half that of $T_{32}$. While validation or development of the existing models [13, 15, 17, 39] is still required for realistic multi-species chemistry, molecular transport and shear generated turbulence extending into the thin reaction zones regime, it appears that they do represent the dominant physics. The remainder of this study focuses on the dissipation rate of other species which do not vary monotonically with progress variable, and for which the existing models are not necessarily applicable.

In contrast with the progress variable dissipation rate, the dissipation rate for intermediate species OH, CO and H is governed by a predominant balance between the reaction term $T_4$ and the dissipation of scalar gradients. The so-called dilatation term $T_2$ appears to be negligible for these species which are weakly correlated with the density. The scalar-turbulence interaction term $T_{32}$ acts to generate scalar gradients, as it did for the progress variable, however its importance is significantly reduced. The dominance of the dissipation-reaction terms results from the intrinsic reaction-diffusion balance present in the structure of premixed flames. The species Damköhler numbers (Table 1) measure the relative chemical time scales, such that the importance of $T_{32}$ is reduced most for the most reactive, highest Damköhler number species, H atom.

**Model development**

The conclusion that intermediate species dissipation rates are controlled by the reaction-diffusion balance in premixed flame structures suggests that flamelet based models for the intermediate species dissipation rates could be used under appropriate conditions. Assuming that the progress variable mixing frequency can be modeled satisfactorily we propose a model that relates it to the mixing frequency for some other reactive scalar $i$. Using $\langle \cdot \mid \zeta \rangle$ to indicate averages conditional on the sample space progress variable $\zeta = c$, and neglecting fluctuations about the conditionally averaged density $\rho_\zeta$ [40], the ratio of mixing frequencies is given by,

$$\frac{\tau_i^{-1}}{\tau_c^{-1}} = \frac{\overline{\rho}\widetilde{\epsilon}_i}{\overline{\rho}\widetilde{\epsilon}_c} \cdot \frac{\widetilde{c''^2}}{\widetilde{Y_i''^2}} = \frac{\widetilde{c''^2}}{\widetilde{Y_i''^2}} \frac{\int_0^1 \rho_\zeta \langle \epsilon_i \mid \zeta \rangle P(\zeta)\, d\zeta}{\int_0^1 \rho_\zeta \langle \epsilon_c \mid \zeta \rangle P(\zeta)\, d\zeta}. \tag{6}$$

If the model is to be used in computations with transported scalar PDFs the scalar variances $\widetilde{c''^2}$, $\widetilde{Y_i''^2}$, the progress variable PDF $P(\zeta)$, and $\rho_\zeta$ are available without further modeling. Closure for the conditional dissipation rate is achieved by expressing the diffusivities and scalar gradients as functions of progress variable,

$$\begin{aligned} \epsilon_c \mid \zeta &\approx \epsilon_c^*(\zeta) = D_c(\zeta)|\nabla c(\zeta)|^2 \\ \epsilon_i \mid \zeta &\approx \epsilon_i^*(\zeta) = D_i(\zeta)|\nabla Y_i(\zeta)|^2. \end{aligned} \tag{7}$$

$D_i(\zeta)$, $D_c(\zeta)$, $\nabla c(\zeta)$ and $\nabla Y_i(\zeta)$ are then obtained from laminar premixed flame solutions. The contribution of mean gradients to the dissipation rate is neglected which is typically an excellent approximation in high Reynolds number flows. The

asterisk is used to denote estimates based directly on the laminar flame structure. Integrating over progress variable space provides initial estimates for the Favre average dissipation rates $\tilde{\epsilon}_i^*$, $\tilde{\epsilon}_c^*$ and mixing frequencies $\tau_i^{*-1}$, $\tau_c^{*-1}$. The scalar gradients used up to this point are exactly those obtained from the laminar flame, although it is known that the gradients in the turbulent flame are subject to turbulence-scalar interactions as discussed in the previous section.

Having obtained $\tau_c^{-1}$, from either an appropriate algebraic model [13, 12, 16, 17] or from solution of a transport equation, the final modeling proposal for the minor species mixing frequencies is,

$$\tau_i^{-1} \approx \frac{\tau_i^{*-1}}{\tau_c^{*-1}} \tau_c^{-1}. \tag{8}$$

Implicit in Eq. 8 are neglect of any intermediate species gradient components which are not aligned with the direction $\mathbf{x}_n$ of the progress variable gradient. Equation 9 indicates that neglecting the possibility that the angle $\alpha$ between $\mathbf{x}_n$ and $\nabla Y_i$ may be finite results in a systematic underestimate of $|\nabla Y_i|$. Scalar alignment characteristics are discussed below.

$$|\nabla Y_i| = \frac{1}{|\cos\alpha|} \left| \frac{\partial Y_i / \partial \mathbf{x}_n}{\partial c / \partial \mathbf{x}_n} \right| |\nabla c|. \tag{9}$$

Additionally it has been assumed in Eq. 8 that any turbulent stretching of the conditional progress variable results in a proportionate change to the intermediate species gradients.

The premises of this modeling approach have been tested using the current DNS data. The laminar flame gradients required have been obtained from strained reactant-versus-product [41] laminar flame calculations with tangential strain rates $a_t$=$0.05\tau_f^{-1}$, $1.5\tau_f^{-1}$ and $3.0\tau_f^{-1}$. The latter strain rates correspond to the mean strain rate conditioned on $\zeta$=0.65 in flames A and C, Table 2. The strain fluctuations of strain rate in these flames are, however, many times greater than the mean values.

A comparison of the conditional flame normal gradients, $\langle \nabla Y_i . \nabla Y_{O2} / |\nabla Y_{O2}| \mid \zeta \rangle$ evaluated from the DNS data, with the gradients observed in strained laminar flames is given in Fig. 4. The $O_2$ flame gradients for both A and C show turbulent flame thickening compared to the laminar solutions. Meanwhile the effect of applying the mean strain rates from flames A and C to the laminar flame is to significantly steepen the $O_2$ gradients. Conversely, strain reduces the magnitude of gradients of intermediate species with peaks within the flame, acting in the same sense as the turbulent flame thickening. The shape of the gradient profiles is best captured by the least strained laminar solution. However, the magnitude of the gradients is not predicted accurately. This indicates that direct use of $\epsilon^*$, found by integrating Eq. 7 over P($\zeta$) is unlikely to be accurate since it does not account for the turbulent stretching and thickening in the flame. Figure 5 shows that the ratio of conditional flame normal gradients, $\langle \nabla Y_i . \nabla Y_{O2} / \nabla Y_{O2} . \nabla Y_{O2} \mid \zeta \rangle$, is modeled by the laminar flame profiles better than the individual $Y_i$ and $Y_{O2}$ gradients. This observation supports the assumption that turbulence-flame interactions modify both the progress variable gradient and the minor species gradients approximately in proportion to one another. Again, the $a_t\tau_f$=0.05 flame provides the best agreement.

The conditionally averaged alignment $\langle \cos(\alpha_i) \mid \zeta \rangle$ between progress variable and the OH, CO, H and $H_2$ gradients is presented in Fig. 6, a magnitude of unity indicates perfect alignment. Each of these quantities peaks in the reaction zone leading to a reversal of the flame alignment. Statistically, the alignment is poor in the preheat layer, where eddies are thought to perturb the flame structure. Focusing of preferentially diffusing species in regions of flame curvature also contributes to the imperfect alignment. Figure 7 shows an instantaneous slice through the progress variable field with iso-lines marking elevated levels of $H_2$ in a region which is concave towards the reactants. The associated gradients parallel to the flame, however are typically much smaller than the peak magnitude of the flame normal gradients for any given species. The neglect of

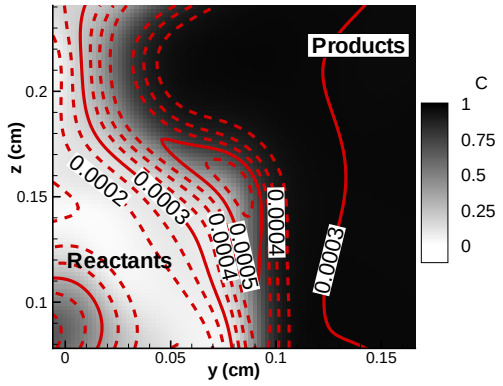


Figure 7: Progress variable contours (greyscale) with $H_2$ iso-lines in the y-z plane at x/$L_x$=0.5, case A.

gradient components normal to the progress variable gradient results in the following approximation for the ratio of conditional dissipation rates,

$$\frac{\langle \epsilon_i \mid \zeta \rangle}{\langle \epsilon_c \mid \zeta \rangle} = \frac{Le_i}{Le_c} \frac{\langle \nabla Y_i . \nabla Y_i \mid \zeta \rangle}{\langle \nabla c . \nabla c \mid \zeta \rangle} \approx \frac{Le_i}{Le_c} \frac{\langle (\nabla Y_i . \nabla c / |\nabla c|)^2 \mid \zeta \rangle}{\langle \nabla c . \nabla c \mid \zeta \rangle}. \tag{10}$$

This ratio and its approximation are plotted in Fig 6 for H only, although similarly good agreement is found for other species. The poor alignment, for example in the preheat layer, does not appear to result in a large difference between the exact and approximate evaluations of the ratio of conditional dissipation rates. The reason may be that occurrences of poor alignment are associated with very low gradients of either progress variable or the other scalar such that they contribute little to the average.

Predictions for the ratios of scalar mixing rates given by Eqs. 6-8 evaluated with the $a_t\tau_f$=0.05 laminar flame solution are compared to the measured values in Fig. 8. The model predicts the shape of the time scale ratio variation correctly at every position shown. At upstream positions the intermediate species mixing rates are greatly over predicted, while excellent agreement is achieved further downstream at x/$L_x$=0.75 where the center line Damköhler number in flame C is 0.47.

The overprediction of the intermediate species mixing rates is associated with the intensely turbulent (lower Damköhler

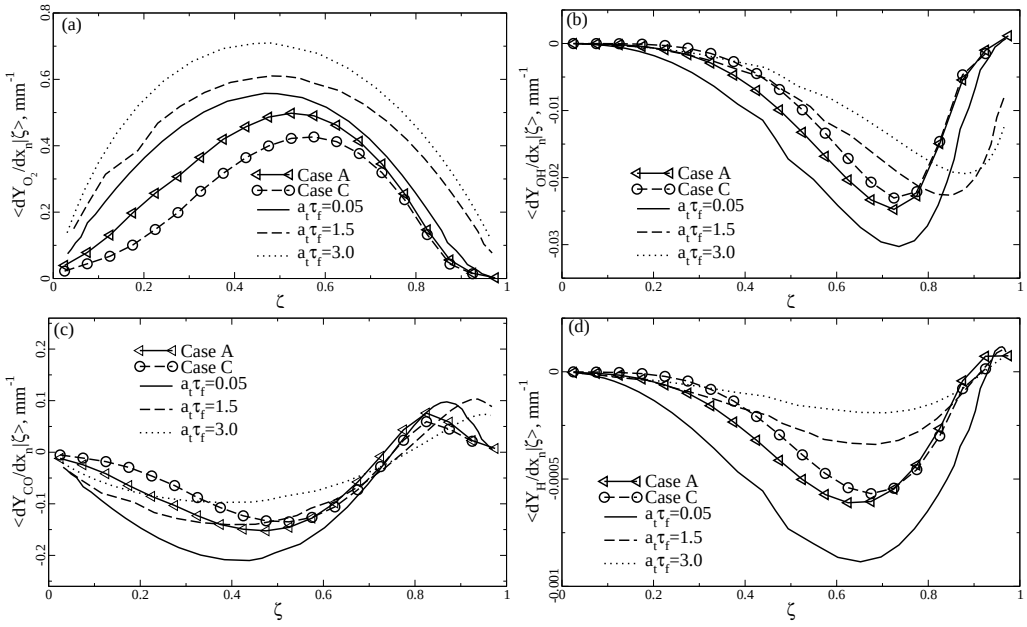


Figure 4: Conditionally averaged flame normal gradient of $O_2$ (a), OH (b), CO (c) and H (d), plotted at $x/L_x$=0.5 for flames A and C. Laminar flame values are shown for $a_t\tau_f$=0.05, 1.5 and 3.0.

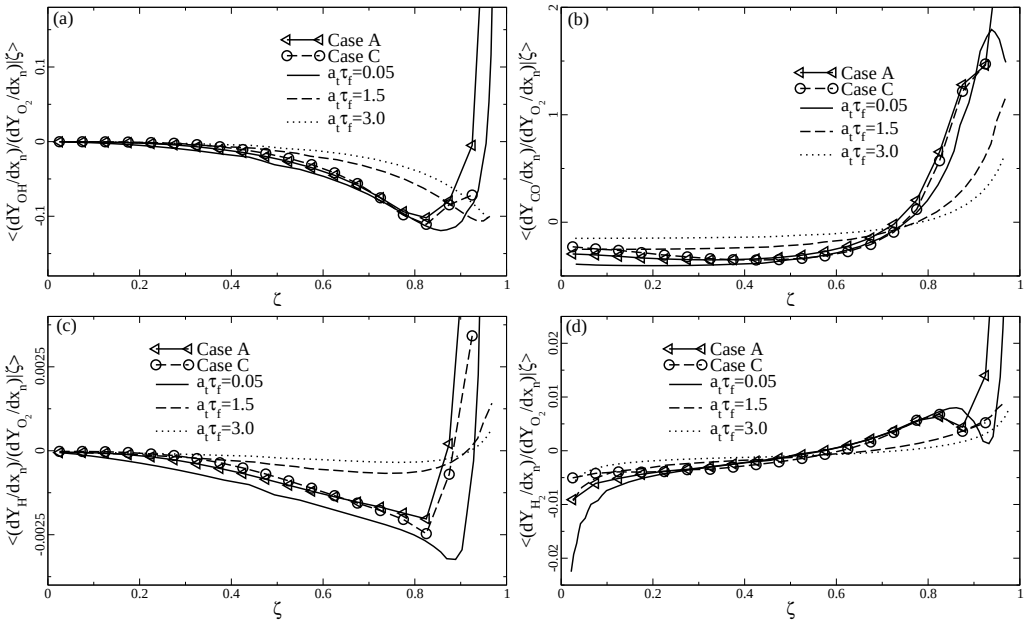


Figure 5: Conditionally averaged flame normal gradient ratios, $\langle \nabla Y_i . \nabla c/|\nabla c| \mid \zeta \rangle$, shown for OH (a), CO (b), H (c) and $H_2$ (d), plotted for $x/L_x$=0.5. Laminar flame values are shown for $a_t\tau_f$=0.05, 1.5 and 3.0.

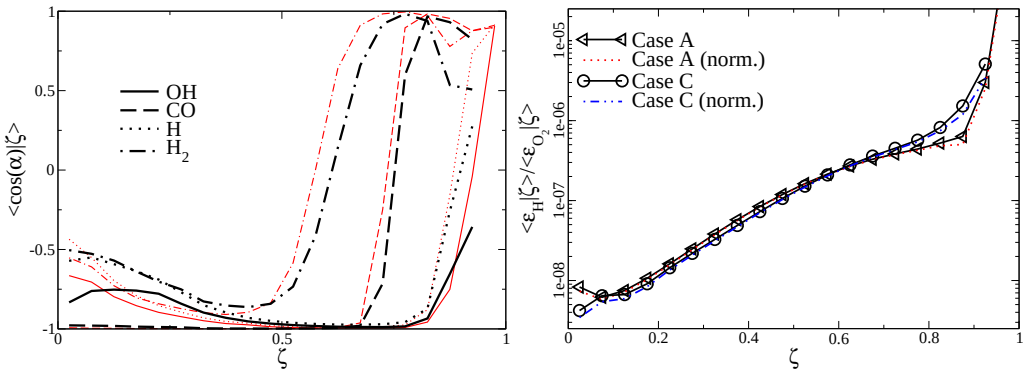


Figure 6: Left: Conditional scalar-progress variable alignment $\langle \cos(\alpha_i) \mid \zeta \rangle$ for OH, CO, H and $H_2$ in flames A (thin red lines) and C (thick black lines). Right: Ratios of the conditional dissipation of H and $O_2$ for flames A and C, and their approximation considering only the flame normal gradients. Data for $x/L_x$=0.5

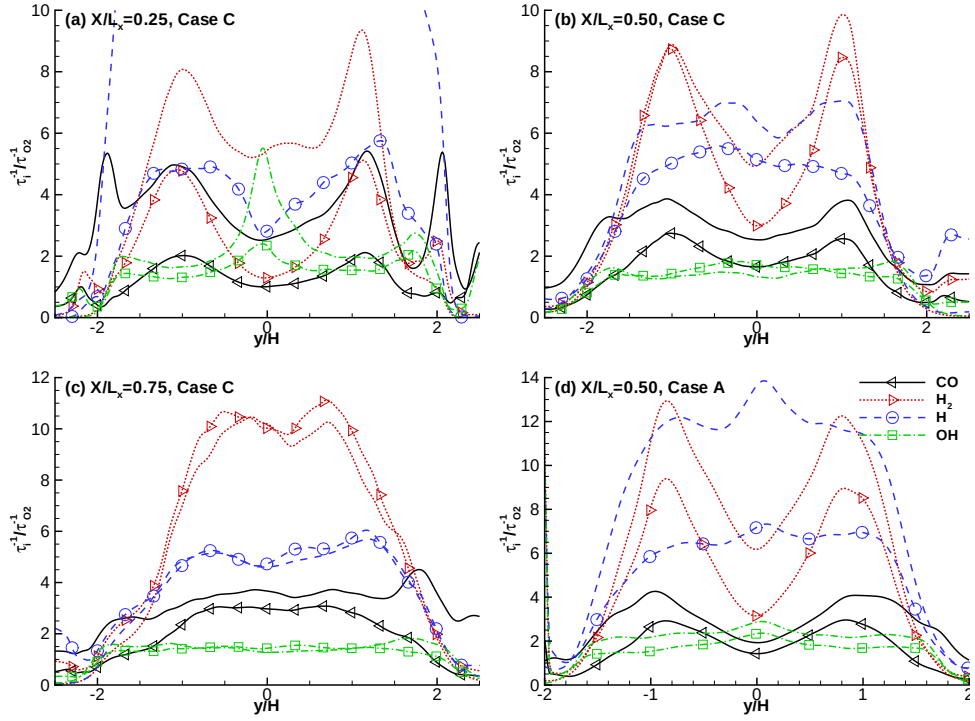


Figure 8: Intermediate species-progress variable time scale ratios showing $\tau_{CO}^{-1}$, $\tau_{H_2}^{-1}$, $\tau_{H}^{-1}$, and $\tau_{OH}^{-1}$ divided by $\tau_{O_2}^{-1}$, comparing predictions of Eqs. 6-8 (no symbols) with DNS measurements (lines with symbols). The variation in the cross stream direction is shown for flame C at $x/L_x$=0.25 (a), $x/L_x$=0.5 (b), $x/L_x$=0.75 (c), and for flame A at $x/L_x$=0.5 (d).

number) region close to the nozzle. The high tangential strain in this region has the effect of decreasing the ratio $\epsilon_i^*/\epsilon_c^*$, Fig. 4, suggesting that use of a more highly strained laminar flamelet would improve predictions. In the low Damköhler number limit passive scalar mixing is recovered and the usual assumption that all species mix at the same rate $\tau_i/\tau_c = 1$ becomes more acceptable. This suggests the use of Damköhler number as an indicator of when the present modeling is valid or when alternative models should be selected. Modeling of scalar mixing rates in the distributed combustion regime is an area requiring further attention.

## Conclusions

The processes governing the progress variable dissipation rate have been analyzed using three-dimensional turbulent Bunsen flame data with reduced methane-air chemistry. The dissipation rate is controlled by a balance between molecular dissipation and gradient generation due to flame propagation, dilatation and compression of scalar gradients by turbulent strain. This confirms previous findings from two-dimensional and simple chemistry analyses.

The mixing rates of intermediate species which do not vary monotonically with progress variable were up to a factor of ten greater than those of progress variable. They are not well modeled by existing models for mixing rates of either the progress variable or of passive scalars. Effects of the so-called dilatation term appear to be negligible for the intermediates. The effect of turbulent straining is also of reduced importance, becoming negligible for the highest Damköhler number species, H atom. Instead, a reaction-dissipation balance dominates the intermediate scalar gradients, driven by the premixed flame structure.

A new model for the ratio of intermediate species and progress variable mixing rates is presented. The model employs the species gradients obtained from laminar flames to estimate the relative magnitude of the species dissipation rates in the turbulent flame. The implied alignment of the species and progress variable provides a good approximation since scalar gradients parallel to the flame make only small contributions to the dissipation rate. The use of laminar flame data also provides a good approximation for the relative magnitude of the species gradients, even in the thin reaction zones regime. Overall, the new model accurately predicts the variation of the intermediate-progress variable mixing frequencies for premixed flame Damköhler numbers greater than 0.5.

## Acknowledgments

The work at SNL was supported by the Division of Chemical Sciences, Geosciences and Bio-sciences, the Office of Basic Energy Sciences (BES), the U.S. Department of Energy (DOE) and also by the U.S. DOE, BES, SciDAC Computational Chemistry program. SNL is a multiprogram laboratory operated by Sandia Corporation, a Lockheed Martin Company, for the U.S. DOE under contract DE-AC04-94-AL85000. This research used resources of the National Center for Computational Sciences (NCCS) at Oak Ridge National Laboratory (ORNL), which is supported by the Office of Science of the U.S. DOE under Contract No. DE-AC05-00OR22725.

## References

[1] S.B. Pope, Prog. Energy Combust. Sci. 11 (1985) 119-192
[2] C. Dopazo, in: P.A. Libby, F.A. Williams (Eds.), Turbulent Reacting Flows, Academic Press, London, 1994, pp. 375-474.
[3] S.B. Pope, Ann. Rev. Fluid Mech. 19 (1987) 237-270.
[4] S. Subramaniam, S.B. Pope, Combust. Flame 115 (1998) 487-514.
[5] E.R. Hawkes, R. Sankaran, J.C. Sutherland, J.H. Chen, Proc. Combust. Inst. 31 (2007) 1633-1640.
[6] R.P. Lindstedt, E.M. Vaos, 145 Combust. Flame (2006) 495-511.
[7] S. Subramaniam, S.B. Pope 117 Combust. Flame (1999) 732-754
[8] S.B. Pope, Turbulent Flows, Cambridge University Press, Cambridge, 2000.
[9] O. Zeman, J.L. Lumley, J. Atmos. Sci. 33 (1976) 1974-1988.
[10] W.P. Jones, P. Musonge, Phys. Fluids 31 (1988) 3589-3604.
[11] T. Mantel, R. Borghi, Combust. Flame 96 (4) (1994) 443-457.
[12] N. Swaminathan, K.N.C. Bray, Combust. Flame 143 (4) (2005) 549-565.
[13] A. Mura, R. Borghi, Combust. Flame 133 (1-2) (2003) 193-196.
[14] G. Hartung, J. Hult, C.F. Kaminski, J.W. Rogerson, N. Swaminathan, Phys. Fluids 20 (2008) 035110.1-16.
[15] N. Chakraborty, N. Swaminathan, Phys. Fluids 19 (2007) 045103.1-10.
[16] N. Chakraborty, N. Swaminathan, Phys. Fluids 19 (2007) 045104.1-11.
[17] A. Mura, K. Tsuboi, T, Hasegawa, Combust. Theory Modelling 12 (4) (2008) 671-698.
[18] T.S. Kuan, R.P. Lindstedt, E.M. Vaos, in: G. Roy (Eds.), Advances in Confined Detonations and Pulse Detonation Engines, Torus Press, Moscow, 2003, pp. 17-40.
[19] P.K. Yeung, S.S. Girimaji, S.B. Pope, Combust. Flame 79 (3-4) (1990) 340-365.
[20] K.N.C. Bray, M. Champion, P.A. Libby, Combust. Flame 127 (1-2) (2001) 2023-2040.
[21] J.H. Chen, H.G. Im, Proc. Combust. Inst. 27 (1998) 819-826.
[22] N. Swaminathan, R.W. Grout, Phys. Fluids 18 (2006) 045102.1-9.
[23] J.-Y. Chen, W.-C. Chang, 133 Combust. Sci. Technol. 133 (4) (1998) 343-375.
[24] C.M. Cha, P. Trouillet, 15 (6) (2003) 1375-1380.
[25] R. Borghi, in: C. Casci (Ed.), Recent Advances in the Aerospace Sciences, Plenum Publishing Corporation, 1985, pp. 117-138.
[26] N. Peters, Turbulent Combustion, Cambridge University Press, Cambridge, 2000.
[27] R. Sankaran, E.R. Hawkes, C.S. Yoo, J.H. Chen, T. Lu, C.K. Law, in: 5th U.S. National Combustion Meeting, 2007 B09.
[28] R. Sankaran, E.R. Hawkes, J.H. Chen, T. Lu, C.K. Law, Proc. Combust. Inst. 31 (1) (2007) 1291-1298.
[29] F. Frenklach, H. Wang, C.-L. Yu, M. Goldenberg, C.T. Bowman, R.K. Hanson, D.F. Davidson, E.J. Chang, G.P. Smith, D.M. Golden, W.C. Gardiner, V. Lissianski, http://me.berkeley.edu/gri_mech.
[30] M.D. Smooke, V. Giovangigli, Lect. Notes Phys. 284 (1991) 1-28.
[31] R.J. Kee, F.M. Rupley, E. Meeks, J.A. Miller, Tech. Rep. SAND96-8216, Sandia National Laboratories, 1996.
[32] T. Passot, A. Pouquet, J. Fluid Mech. 181 (1987) 441-466.
[33] T.J. Poinsot, S.K. Lele, J. Comp. Phys. 202 (1992) 104-139.
[34] J.C. Sutherland, C.A. Kennedy, J. Comp. Phys. 191 (2003) 502-524.
[35] C. Yoo, Y, Wang, A. Trouvé, H. Im, Combust. Theory Modelling 9 (4) (2005) 241-260.
[36] C.S. Yoo, H.G. Im, Combust. Theory Modelling 11 (2) (2007) 259-286.
[37] C.A. Kennedy, M.H. Carpenter, Appl. Numer. Math. 14 (4) (1994) 397-433.
[38] C.A. Kennedy, M.H. Carpenter, R.M. Lewis, Appl. Numer. Math. 35 (2000) 177-219.
[39] K.N.C. Bray, N. Swaminathan, Comptes Rendus Mècanique 334 (8-9) (2006) 446-473.
[40] N. Swaminathan, R.W. Bilger, B. Cuenot, Combust. Flame 126 (4) (2001) 1764-1779.
[41] A.E. Lutz, R.J. Kee, J.F. Grcar, F.M. Rupley, Tech. Rep. SAND96-8243, Sandia National Laboratories, 1996.